NsG-352

Exciton and Impurity States in Rare Gas Solids*+

J. Hermanson++
University of Chicago
Institute for the Study of Metals
and
Department of Physics
Chicago, Illinois 60637

32436

Abstract

The formalism of the preceding paper is applied to a calculation of the first excited states of (1) pure crystals of Kr and Xe; and (2) rare gas solids containing a substitutional Xe impurity. A Hartree potential for the bare electron-hole interaction is constructed for each system, and is screened within the random phase approximation. Matrix elements of the corresponding pseudopotentials, projected according to the Cohen-Heine prescription, are derived in the Wannier representation. Band structures inferred from optical data are fitted to simple interpolation formulae. By transformation to a symmetric representation for the envelope function, the Wannier difference

equations are reduced to manageable form and solved by a matrix technique. Although the calculations contain no disposable parameters, obtained binding energies and oscillator strengths are found to be in excellent agreement with experiment.

---

*Supported in part by ONR, NSF, NASA, and a general grant to ISM by ARPA.

+Submitted in partial fulfillment of the requirements for the Ph.D. degree at the University of Chicago.

++Xerox Fellow, 1965-66.

1. Introduction.

In the preceding paper[1] the wave-packet theory of exciton and impurity states developed by Wannier and other workers was reviewed. It was asserted that the wave-packet approach, which has been supposed to be valid only for shallow states, in fact could be made to yield satisfactory results for deep states as well, providing that certain microscopic modifications of the customary macroscopic theory were introduced. The purpose of this paper is to examine this statement in detail for the simplest systems containing deep exciton and impurity states, viz., the solid rare gases. For these systems the calculations turn out to be unexpectedly easy, and the results in excellent agreement with experiment. The extension of the methods to other crystals appears to be straightforward.

We begin our presentation in section 2 with an approximate treatment of dielectric screening of the electron-hole interaction in solid rare gases. In section 3 we describe the construction of complete pseudopotentials for the systems studied. Kinetic energy terms arising from the periodic crystal potential are discussed in section 4, which is followed by a reduction of the Wannier difference equations in section 5. Sections 6 and 7 contain a discussion of the results and comparison with experiment.

2. Dielectric Model for Isotropic Insulators.

In section 4 of I we noted that the Fourier components $V_s(q)$ of the self-consistent potential acting between external charges are given by

$$V_s(q) = V_b(q) \Big/ \varepsilon(q, K=0) \tag{2.1}$$

where $V_b(q)$ is the Fourier transform of the bare potential. The dielectric function neglecting local field effects is[2]

$$\varepsilon(q, K=0) = 1 + \frac{4\pi e^2}{q^2} \sum_{mn\,\underline{k}} \frac{|\langle n\,\underline{k}+\underline{q}\,|\, e^{i\underline{q}\cdot\underline{r}} \,|\, m\,\underline{k}\rangle|^2}{W_n(\underline{k}+\underline{q}) - W_m(\underline{k})} \tag{2.2}$$

for insulating crystals, where W_n and W_m are electron and hole band energies, respectively, and

$$\langle n\,\underline{k}+\underline{q}\,|\, e^{i\underline{q}\cdot\underline{r}} \,|\, m\,\underline{k}\rangle = \Omega^{-1} \int d\underline{r}\, \varphi^*_{n\,\underline{k}+\underline{q}}(\underline{r})\, e^{i\underline{q}\cdot\underline{r}}\, \varphi_{m\,\underline{k}}(\underline{r}) \tag{2.3}$$

is a transition matrix element connecting the Bloch states $\varphi_{m\underline{k}}$ and $\varphi_{n\underline{k}+\underline{q}}$; m and n are valence and conduction band indices, respectively, and Ω is the volume of the unit cell. Equation (2.2) corresponds to virtual excitations of electron-hole pairs of momentum q and energy

$$E_{mn}(\underline{k}, \underline{k}+\underline{q}) = W_n(\underline{k}+\underline{q}) - W_m(\underline{k}) \tag{2.4}$$

For solid rare gases only the outer np valence shell need be included in the summation on m in (2.2), since the other shells are more tightly bound, with negligible polarizabilities. Moreover, conduction band widths in the rare gases are nearly equal to their free-electron values[3]; hence, we may replace the $\psi_{n\underline{k}}$ by plane waves, as a first approximation (comparison of the calculations of $\mathcal{E}(q,0)$ by Penn[4] and Nara[5] for Si shows that exact representation of the $\psi_{n\underline{k}}$ is not crucial). Then the matrix element of $e^{i\underline{q}\cdot\underline{r}}$ is given by the Fourier transform of an np orbital, which decreases sharply for wave vectors not contained in the central Brillouin zone. Thus we may use a two-band model for the polarization, corresponding to retaining only np $\longrightarrow$ (n+1)s atomic excitations; oscillator strengths are adjusted to satisfy the sum rule[6]

$$\sum_n |\langle n\,\underline{k}+\underline{q}|\, e^{i\underline{q}\cdot\underline{r}}\,|m\,\underline{k}\rangle|^2 E_{mn}(\underline{k},\underline{k}+\underline{q}) = \frac{\hbar^2}{2m} q^2 \qquad (2.5)$$

With $\underline{k}$ restricted to the first zone, we obtain the approximate result

$$\varepsilon(q0) = 1 + \frac{2\pi\hbar^2 e^2}{m} \sum_{\underline{k}} \left[E_{mn}(\underline{k},\underline{k}+\underline{q})\right]^{-2} \qquad (2.6)$$

An important characteristic of rare gas crystals is the large energy gap between valence and conduction bands. This has the effect of reducing the sensitivity of (2.6) both to the shape of the bands and the approximations made to the oscillator strengths. In addition the valence electron overlap is small, so that the valence bands have small width. For our purposes it is sufficient to represent the pair excitation energies by a free electron model with a large "zero of the energy". Thus we may write

$$E_{mn}(\underline{k},\underline{k}+\underline{q}) = E_G + \frac{\hbar^2}{2m}(\underline{k}+\underline{q})^2 \qquad (2.7)$$

where E_G is the band gap. Substituting (2.7) into (2.6), we obtain

$$\varepsilon(q0) = 1 + \frac{8\pi me^2}{\hbar^2}\sum_{\underline{k}}\left[(\underline{k}+\underline{q})^2 + k_0^2\right]^{-2} \qquad (2.8)$$

where $k_0^2 = 2mE_G/\hbar^2$. In terms of the static dielectric constant ε_0 the isotropic part of $\varepsilon(q0)$ is given by

$$\varepsilon(q0) = 1 + (\varepsilon_0 - 1)\Sigma(q)/\Sigma(0) \qquad (2.9)$$

where

$$\Sigma(q) = \tan^{-1}\left(\frac{K+q}{k_0}\right) + \tan^{-1}\left(\frac{K-q}{k_0}\right) - \frac{k_0}{2q}\log\left[\frac{(K+q)^2+k_0^2}{(K-q)^2+k_0^2}\right]$$

Here K is the average "radius" of the Brillouin zone, given by

$$\frac{4\pi}{3} K^3 = 8\pi^3/\Omega$$

Equation (2.9) is shown in Fig. 1 as a function of wave number q for Ar; similar results are obtained for the other rare gases.

Our model for an isotropic insulator differs somewhat from Penn's model for an isotropic semiconductor[4]. The values obtained from his interpolation formula (with the parameters adjusted to Ar) are also shown in Fig. 1. In both models $\varepsilon \to 1$ when $q \to \infty$, while $\varepsilon \to \varepsilon_0$ as $q \to 0$. Consequently there is no screening of the electron-hole interaction for r = 0, while $\varepsilon(r) \to \varepsilon_0$ for large r, in agreement with macroscopic considerations[7]. The scale of the breakdown region in real space may be determined from the definition of $\varepsilon(r)$:

$$\frac{1}{\varepsilon(r)} \frac{e^2}{r} = P \int \frac{dq}{(2\pi)^3} \frac{1}{\varepsilon(q_0)} w(q) e^{iq \cdot r} \qquad (2.10)$$

where $w(q) = 4\pi e^2/q^2$

is the Fourier transform of the Coulomb potential and P denotes the principle part. In order to simplify the integration

of (2.10) we replace (2.9) by the simpler function

$$F(q) = 1 + (\varepsilon_0 - 1)\,\alpha^2 K^2/(q^2 + \alpha^2 K^2) \quad ;$$

α is chosen to provide a good fit to $\varepsilon(q,0)$ and is of order unity for the rare gases. After a trivial contour integration we find the result

$$\frac{1}{\varepsilon(r)} = \frac{1}{\varepsilon_0} + \frac{\varepsilon_0 - 1}{\varepsilon_0} \exp(-Qr) \tag{2.11}$$

where $Q = \varepsilon_0^{1/2} \alpha K$. We note that because E_G is large the breakdown length Q^{-1} is less than the atomic radius. Then $\varepsilon(r)$ may be replaced by ε_0 outside the central cell. Within the core region of the "impurity" the simple RPA result is not expected to be valid. On the other hand, the excited electron has almost no amplitude in the region since it must be orthogonal to the core levels (cf. I, section 3). Thus, local field effects can be neglected, and we may write for all r

$$V_s(\underline{r}-\underline{R}_i) = V_b(\underline{r}-\underline{R}_i)/\varepsilon(r) \tag{2.12}$$

where $V_b(\underline{r}-\underline{R}_i)$ is the unscreened potential.

3. Impurity Potentials.

Exciton and impurity states satisfy a generalized impurity equation (See I, section 2)

$$(K_o + V'(\underline{r}-\underline{R}_i))\,\psi(\underline{r}-\underline{R}_i) = E\,\psi(\underline{r}-\underline{R}_i) \qquad (3.1)$$

where K_o has full crystal symmetry and V' is an appropriate impurity potential centered about $\underline{R}_i$.

By working in a representation based on the smooth part of ψ (See I, section 3), we found that (3.1) could be rewritten as

$$(K^o_{ps} + V'_{ps}\ (\underline{r}-\underline{R}_i))\,\varphi(\underline{r}-\underline{R}_i) = E\,\varphi(\underline{r}-\underline{R}_i) \qquad (3.2)$$

where K^o_{ps} is the pseudopotential kinetic energy operator for the perfect crystal and V'_{ps} is the "impurity pseudopotential". The smooth function φ is given by

$$\psi = \varphi - \sum_t \phi_t \langle \phi_t | \varphi \rangle \qquad (3.3)$$

in terms of the core functions ϕ_t. Because V'_{ps} is small in the cores, interband matrix elements are sharply reduced, so that a one-band approximation for φ is possible. In terms of Wannier functions $\alpha_{n\underline{R}}$ derived from K^o_{ps}, we may write

$$\varphi(\underline{r}-\underline{R}_i) = \sum_{\underline{R}} F(\underline{R})\, \alpha_{n\underline{R}}(\underline{r}-\underline{R}_i) \qquad (3.4)$$

where n denotes the first conduction band. Inserting (3.4) into (3.2) we have

$$\sum_{\underline{R}'} \left\{ W(\underline{R}-\underline{R}') - E\,\delta_{\underline{R}\underline{R}'} + V(\underline{R},\underline{R}') \right\} F(\underline{R}') = 0 \qquad (3.5)$$

where

$$W(\underline{R}-\underline{R}') = \left\langle n\underline{R} \middle| K^{o}_{ps} \middle| n\underline{R}' \right\rangle \qquad (3.6)$$

and

$$V(\underline{R},\underline{R}') = \left\langle n\underline{R} \middle| V'_{ps} \middle| nR' \right\rangle$$

are matrix elements of the crystal and impurity pseudopotentials in the α-representation. The model Wannier equation (3.5) are the fundamental equations we wish to solve. The method of solution consists of three steps: (1) we construct a pseudopotential for each system, (2) we compute the matrix elements (3.6), and (3) we solve the secular equation

$$\det \| W(R-R') - E\,\delta_{\underline{R}\underline{R}'} + V(\underline{R},\underline{R}') \| = 0 \quad ; \qquad (3.7)$$

the model amplitude functions $F(\underline{R})$ are determined from (3.5). Let us now turn to the calculation of the pseudopotentials.

The impurity potential for a crystal containing a positively charged ion at $\underline{R}_i$ is

$$V_o(\underline{r}-\underline{R}_i) = V_{ion}(\underline{r}-\underline{R}_i) - V_{host}(\underline{r}-\underline{R}_i) \tag{3.8}$$

where V_{ion} is the screened potential of the ion and V_{host} is the potential of a neutral host atom. The analogous potential for exciton states was derived in I. Because of the tight binding of rare gas atoms we neglect the motion of the hole; then the exciton potential may also be written in the form (3.8). V'_{ps} is given by the Cohen-Heine prescription[8]:

$$V'_{ps}\,\varphi = V_o\varphi - \sum_t \phi_t \langle \phi_t | V_o | \varphi \rangle \tag{3.9}$$

Because φ is slowly varying in the core region we make the local approximation

$$\begin{aligned} V'_{ps} &= V_o - \sum_t \phi_t \langle \phi_t | V_o \rangle \\ &= V_o + V_R \end{aligned} \tag{3.10}$$

A convenient prescription for including polarization effects in the impurity potential was given in section 2 in terms

of a bare potential $V_b(r)$ and a dielectric constant $\mathcal{E}(r)$. We construct a Hartree potential for V_b:

$$V_b(r) = u_{ion}(r) - u_{host}(r) \tag{3.11}$$

where

$$u_{ion}(r) = -\frac{Z_1 e^2}{r} + e^2 \sum_s' \int d\underline{r}' \frac{|\phi_s^{(1)}(\underline{r}')|^2}{|\underline{r}-\underline{r}'|} \tag{3.12a}$$

and

$$u_{host}(r) = -\frac{Z_o e^2}{r} + e^2 \sum_s \int d\underline{r}' \frac{|\phi_s^{(0)}(\underline{r}')|^2}{|\underline{r}-\underline{r}'|} \tag{3.12b}$$

are ionic and atomic potentials, neglecting exchange and polarization effects. Z_o and Z_1 denote the atomic number of the host and impurity atoms, while $\phi_s^{(o)}$ and $\phi_s^{(1)}$ are the corresponding core orbitals taken from free atom calculations[9]. One np orbital is deleted from the sum in (3.12a) so that $u_{ion} \sim r^{-1}$ for large r. The self-consistent potential V_o was derived from equation (2.12) for each system, and pseudopotentials V_{ps}' were calculated from (3.10). The unscreened pseudopotential for excitonsin Xe is shown in Fig. 2, along with the hydrogenic potential

$$V_H'(r) = -\frac{e^2}{r} \tag{3.13}$$

As we expected (cf. I) V'_{ps} is greatly reduced in the core region, and approaches the Coulomb law (3.13) outside the cores (the addition of dielectric screening modifies V'_{ps} somewhat). Similar results were found for the other systems.

Before we can solve (3.7) we must compute matrix elements of V'_{ps} in the α -representation. According to I we have

$$\alpha_{n\underline{R}} = N^{-1/2} \sum_{\underline{k}} e^{i\underline{k}\cdot\underline{R}} \varphi_{n\underline{k}} \tag{3.14}$$

where $\varphi_{n\underline{k}}$, the smooth part of a Bloch funtion $\psi_{n\underline{k}}$, is an eigenfunction of K^o_{ps}:

$$K^o_{ps} \varphi_{n\underline{k}}(\underline{r}) = W_n(\underline{k}) \varphi_{n\underline{k}}(\underline{r}) \tag{3.15}$$

Because the band structure $W_n(\underline{k})$ is approximately given by a free-electron formula[3] we may approximate $\varphi_{n\underline{k}}$ by a plane wave

$$\varphi_{n\underline{k}} = V^{-1/2} \exp(i\, \underline{k}\cdot\underline{r}) \tag{3.16}$$

(This will not be true of $\psi_{n\underline{k}}$, which must contain an admixture of core functions). We calculate (3.14) by approximating the first Brillouin zone by a sphere of the same volume

(Wigner-Seitz approximation). This leads easily to the result

$$\alpha_{n\underline{R}}(\underline{r}) = \frac{1}{2\pi^2\sqrt{\Omega}} \left(\frac{\sin K\rho - K\rho\cos K\rho}{\rho^3} \right) \tag{3.17}$$

where $\rho = |\underline{r}-\underline{R}|$ and K is given by

$$\frac{4\pi}{3} K^3 = (2\pi)^3/\Omega$$

; (3.17) is spherically symmetric about r = R.

We are now in a position to calculate the potential energy terms in the difference equations. According to equations (3.6) these are given by

$$V(\underline{R},\underline{R}') = \int d\underline{r}\ \alpha^{*}_{n\underline{R}}(\underline{r})\, V'_{ps}(\underline{r})\, \alpha_{n\underline{R}'}(\underline{r}) \tag{3.18}$$

Because of the orthogonality of Wannier functions centered about different sites, off-diagonal elements of $V(\underline{R},\underline{R}')$ are small for large R, and will be neglected. In addition, the diagonal elements must approach the hydrogenic formula $-e^2/\varepsilon_o R$ for R sufficiently large that V'_{ps} may be assumed constant over a unit cell.

There are three matrix elements for which the continuum approximation

$$(\underline{R}|V'_{ps}|\underline{R}') = \left(-e^2/\varepsilon_o R\right) \delta_{\underline{R}\underline{R}'} \tag{3.19}$$

is not suitable. These are

(1) The one-center term $\langle 0|V'_{ps}|0\rangle$ (diagonal central cell correction);

(2) The two-center nearest neighbor charge-transfer term $\langle 0|V'_{ps}|d\rangle$, and

(3) The dipolar nearest neighbor term $\langle d|V'_{ps}|d\rangle$.

Values of these matrix elements are given in table I for $V = V'_{ps} = V_o + V_R$. Also shown are values of these quantities computed without orthogonality corrections ($V = V_o$), along with values of $e^2/\mathcal{E}_o d$. We note that all matrix elements are substantially reduced by the inclusion of V_R in the impurity potential, and that the reduction is greatest when the size disparity between impurity and host atoms is greatest (Xe in Ne). These "excluded volume effects" will be shown below to play a dominant role in interpreting the observed trends in binding energies and oscillator strengths.

4. Interband Kinetic Energy.

The kinetic energy terms $W(\underline{R}-\underline{R}')$ of equation (3.5) are, in terms of the band structure of the host lattice,

$$W(\underline{R}-\underline{R}') = N^{-1} \sum_{\underline{k}} [W_n(\underline{k}) - W_m(\underline{k})]\, e^{i\,\underline{k}\cdot(\underline{R}-\underline{R}')} \qquad (4.1)$$

where $W_n(\underline{k})$ and $W_m(\underline{k})$ are band structures for the electron and hole respectively (we set $W_m(\underline{k})$ equal to a constant for impurity states or trapped excitons) and the $\underline{k}$-space sum is restricted to the first Brillouin zone. In figure 3 we show the band structure of solid Xe as inferred[3] from Baldini's optical data. The important features are the flat valence bands, the wide conduction band, and the large spin-orbit splitting in the valence bands. In order to simplify the calculation of $W(\underline{R}-\underline{R}')$ we employ an interpolation model for the band structure:

$$W_n(\underline{k}) - W_m(\underline{k}) = E_G + \frac{E_L}{3}\left[3-\cos\left(\frac{ak_x}{2}\right)\cos\left(\frac{ak_y}{2}\right) - \cos\left(\frac{ak_x}{2}\right)\cos\left(\frac{ak_z}{2}\right) - \cos\left(\frac{ak_y}{2}\right)\cos\left(\frac{ak_z}{2}\right)\right] \quad (4.2)$$

where a is the lattice parameter, E_G the energy gap and E_L the band width at L.

According to Phillips' nearly free electron model for the conduction bands,[10]

$$\begin{aligned} E_L &= E_f(L) - S_L/2 \\ &= \frac{3h^2}{8ma^2} - S_L/2 \end{aligned} \quad (4.3)$$

where $E_f(k) = \hbar^2k^2/2m$ and S_L is the nearly free electron

splitting of the L_1 and L_2, levels. In Xe $E_f(L)$ is 2.9 eV and S_L determined spectroscopically is 1.4 eV, so that E_L is 2.2 eV. Spectroscopic data to determine S_L are not available for Ne, Ar or Kr.

To determine S_L in these crystals we make use of the chemical trends in s-p splittings which are manifested in several ways. In the alkali metals[11] the s-p splitting at $\underline{k} = \underline{N}$ decreases from Li to Cs, reversing sign between Na and K. Also low-energy electron scattering from rare gas atoms is characterized[12] by the lengths f_o shown in Table II. Again a sign reversal occurs, and in the atoms adjacent to those for which the alkali s-p splitting reverses sign. Thus we assume that S_L vanishes for Ne and interpolate linearly between Ne and Xe to obtain the Ar and Kr values also shown in Table II. Note that although (4.2) has the <u>form</u> of a tight-binding expansion, the parameter E_L is determined primarily by $E_f(L)$, as can be seen in Table II, and not by interatomic overlap integrals.

The tight-binding form assumed for (4.2) reduces near $\underline{k} = 0$ to const. + $E_L(ka)^2/12$ or const. + $(\hbar k)^2/2\mu$ with μ/m listed in Table II. These values of μ/m disagree significantly with the continuum values of μ^*/m deduced by Baldini from a hydrogenic model of the n = 2,3 levels.[13] It is evident that our single parameter E_L cannot reproduce

both the band width and $(\mu^*)^{-1}$, the curvature near k = 0, correctly. A correction is made for this deficiency in the calculations discussed later.

5. Reduction of Wannier Equations.

It is convenient to transform to a representation based on symmetrized linear combinations of the $\alpha_{n\underline{R}}$. Any two of the transformed basis functions have vanishing matrix elements coupling them unless both functions have the same symmetry under an appropriate subgroup of the point group of the crystal; thus the secular equation may be factorized into sets of equations having lower dimensionalities. The correct symmetry group may be determined from inspection of the Wannier equations (3.5). Each interband edge may generate bound states; if the interband edge is degenerate (as in many-valley semiconductors), supermultiplets will be formed which will exhibit a so-called valley-orbit splitting consistent with that subgroup of the full point group which interchanges the band edges.

Fortunately in rare gas solids by neglecting the valence band width we can deal with a non-degenerate interband edge at $\underline{k} = \Gamma = 0$ for both excitons and impurities. We are interested only in s exciton states because the transition $\Gamma_{15} \longrightarrow \Gamma_1$ is dipole allowed. Similarly for the

impurity states we calculate only s states and assume that ns and np states of the impurity are degenerate, so that ls $\longrightarrow$ np excitation energies can be obtained from a knowledge of the positions of the s levels alone.

The s states are the totally symmetric linear combinations γ_s of the Wannier functions $\alpha_{\underline{R}}$:

$$\gamma_s(\underline{r}) = N_s^{-1/2} \sum_{\underline{R}_s} \alpha_{\underline{R}_s}(\underline{r}) \tag{5.1}$$

where the sum is over lattice vector belonging to the s^{th} "star" containing N_S members, and we have

$$\varphi(\underline{r}-\underline{R}_i) = \sum_s G_s \gamma_s(\underline{r}-\underline{R}_i) \tag{5.2}$$

where $G_S = \sqrt{N_S}\ F(|\underline{R}_S|)$

It is easy to show that the transformation (5.1) is unitary. Equations (3.5) are replaced by

$$\sum_{S'} H_{SS'} G_{S'} = E G_S \ , \tag{5.3}$$

where $H_{SS'} = W_{SS'} + V_{SS'}$ with the definitions

$$W_{SS'} = (N_S N_{S'})^{-1/2} \sum_{\underline{R}_S \underline{R}_{S'}} W(\underline{R}_S - \underline{R}_{S'}) \tag{5.4a}$$

$$V_{SS'} = (N_S N_{S'})^{-1/2} \sum_{\underline{R}_S \underline{R}_{S'}} V(\underline{R}_S, \underline{R}_{S'}) \tag{5.4b}$$

In this " γ -representation" we have one basic function for each distinct star of lattice vectors, and the dimensionality of the secular equation is reduced by a factor of about 20. An expansion of φ out to 30 or 40 shells is now possible, so that this formalism is appropriate to the study of "intermediate" excitons (e.g., in alkali halides and rare gas solids). Recalling the identity

$$N^{-1} \sum_{\underline{k}} e^{i\,\underline{k}\cdot(\underline{R}-\underline{R}')} = \delta_{\underline{R},\underline{R}'}$$

it is easy to show that

$$W_{SS'} = \sum_{S''} A_{S''} \sum_{\underline{R}_S \underline{R}_{S'},\underline{R}_{S''}} \delta_{\underline{R}_{S''},\underline{R}_S-\underline{R}_{S'}} \qquad (5.5)$$

where A_S is defined in the expansion

$$W_n(\underline{k}) - W_m(\underline{k}) = \sum_S A_S \left(N_S^{-1/2} \sum_{\underline{R}_S} e^{i\,\underline{k}\cdot\underline{R}_S} \right) \qquad (5.6)$$

The expansion (5.9) is always possible because of the continuity and cubic symmetry of $(W_n - W_m)$. In our tight-binding model there are only two non-vanishing coefficients A_S, representing the energy gap and the band width. Equation (5.8) for the kinetic energy terms is convenient because it contains no $\underline{k}$-space integration (see equation (4.1)). As before, the energy gap appears only along the diagonal ($S = S'$) and may be set equal to zero; then $W_{SS'}$ is linear in E_L

(the lattice sums in (5.8) depend only upon crystal symmetry). Since E_L decreases with increasing atomic number, the density of states at the interband edge increases with Z, which in turn has the effect of enhancing binding energies for large Z. This trend, however, is reversed by the Z-dependence of ε_o, which increases[13,14] from 1.1 for Ne to 2.23 for Xe.

6. Excitons in Xe and Kr.

We are now in a position to solve the Wannier difference equations (3.5) using both a realistic band structure and an interaction which include three corrections to the hydrogenic problem:

(1) Breakdown of macroscopic dielectric screening in the central cell (DB),

(2) Non-parabolic energy bands (KE), and

(3) Repulsive terms in the central cell (R).

Corrections (1) and (2) were previously considered by Kohn and Luttinger[15]; when $m^*/m \ll 1$ both corrections produce negative shifts of the 1s energies below their hydrogenic values. Correction (3) arises from the orthogonality terms discussed in the preceding paper.

Before solving the difference equations carefully we wish to illustrate the relative magnitude of these three terms by solving a model differential equation, treating

these effects by first-order perturbation theory. We know that for the exciton states the hydrogenic model works very well. Our unperturbed wave function is therefore the hydrogenic 1s state described by Baldini[13]:

$$\psi_{1s}(r) = \left(\frac{\pi}{a_o}\right)^{3/2} e^{-r/a_o} \tag{6.1}$$

where $a_o = \frac{\hbar^2}{me^2}\left(\frac{\varepsilon_o}{\mu^*/m}\right)$ is the first Bohr radius according to the effective mass approximation[16] (EMA). We construct a model Hamiltonian which contains, in a qualitative way, the effects due to DB, KE, and R:

$$H_M = K_M + V_M' \tag{6.2}$$

The kinetic energy operator

$$K_M = -\frac{\hbar^2}{2m} \cdot \frac{1}{2}\left\{\frac{m}{\mu(r)}\nabla^2 - \nabla^2\frac{m}{\mu(r)}\right\} \tag{6.3}$$

contains the effects of large-k variation of μ^*; $\mu(r)$ is a radially-dependent effective mass described below. Corrections due to dielectric breakdown and repulsive terms in the central cell are contained in a model potential

$$V_M' = \frac{-e^2}{\varepsilon(r)r}\left[1 - \theta(r-r_o)\right] \tag{6.4}$$

Except for the radial dependence of the dielectric constant, V_M' is a hydrogenic potential for $r > r_o$; we assume that cancellation between V' and V_R' is exact for $r < r_o$, the radius of the "excluded volume".

Interpolation formulae were constructed for the radial dependences of $\mu(r)$ and $\varepsilon(r)$. The formulae give correct limiting behavior for $r \rightarrow \infty$ and $r \rightarrow 0$, with exponential interpolation between the limits, characterized by decay factors which scale with the lattice constant. Variation of the dielectric constant was chosen to be of the form

$$\frac{1}{\varepsilon(r)} = \frac{1}{\varepsilon_o} + \left(\frac{\varepsilon_o - 1}{\varepsilon_o}\right) \exp(-Qr) \qquad (6.5)$$

where $Q = K_F$ is the Fermi wave number. Note that $\varepsilon(r)$ approaches 1 for small r and ε_o for large r, and that Q^{-1} plays the role of a characteristic breakdown length for an insulator. Qualitatively the variation of effective mass (in real space) can be described in terms of μ^*, the macroscopic ($k \rightarrow 0$) effective mass, by

$$\frac{m}{\mu(r)} = \frac{m}{\mu^*} - \left(\frac{m}{\mu^*} - 1\right) \exp\left[-r/a\right] . \qquad (6.6)$$

For small r, $\mu(r)$ tends to the free electron value m, whereas $\mu(r) \rightarrow \mu^*$ as $r \rightarrow \infty$. Note that r = a is associated with wave number $k = \frac{2\pi}{a}$, so that a^{-1} is a characteristic

decay factor for the effective mass. The pertinent microscopic quantities Q and a^{-1} are given in Table III. Also shown is a third parameter $\gamma = r_o/A$ the equivalent radius of the excluded volume according to first-order perturbation theory, relative to the atomic radius A (see equation (6.4)).

With the above interpolation formulae the model Hamiltonian (6.2) can be written as

$$H_M = H_{EMA} + H_{CC} \tag{6.7}$$

where $H_{EMA} = -\frac{\hbar^2}{2\mu^*}\nabla^2 - \frac{e^2}{\varepsilon_o r}$ is the macroscopic Hamiltonian[16], and

$$H_{CC} = V_{DB} + V_{KE} + V_R$$

contains the central cell corrections. Here

$$V_{DB} = -\left(\frac{\varepsilon_o - 1}{\varepsilon_o}\right) \frac{e^2}{r}\left[1 - \theta(r-r_o)\right]\exp\ [-Qr] \tag{6.8a}$$

represents dielectric breakdown for $r > r_o$ and vanishes for $r < r_o$; corrections for the non-parabolic nature of the energy

bands are contained in the term

$$V_{KE} = -\frac{\hbar^2}{2m}\left(\frac{m}{\mu^*} - 1\right)\left\{\frac{\exp(-r/a)\nabla^2 + \nabla^2\exp(-r/a)}{2}\right\} \tag{6.8b}$$

and

$$V_R = \frac{e^2}{\epsilon_o r}\,\theta\,(r-r_o) \tag{6.8c}$$

is the effective (local) repulsive potential.

We are now in position to calculate the first-order corrections to the hydrogenic theory. According to the Kohn-Luttinger model the energy shift is[15]

$$\Delta E_{KL} = \langle V_{DB} \rangle + \langle V_{KE} \rangle \tag{6.9}$$

whereas according to the theory of the preceding paper,

$$\Delta E = \langle V_{DB} \rangle + \langle V_{KE} \rangle + \langle V_R \rangle \,. \tag{6.10}$$

The calculated shifts $\langle V_{DB} \rangle$, $\langle V_{KE} \rangle$ and $\langle V_R \rangle$ are given in Table IV, along with ΔE_{KL} and the total shift ΔE, for 1s excitons in Kr and Xe. The experimental shifts are presented in the same table. We see that the positive

contribution, $\langle V_R \rangle$, is large, and that in spite of considerable cancellation the predicted shifts agree in sign with the rather small hydrogenic defects for both crystals. Thus, the unexpected success of the EMA for excitons in Kr and Xe is due to the substantial cancellation between central cell corrections.

We expect generally that the hydrogenic theory will be useful for deep exciton states in other filled-shell insulators such as alkali halides. For deep impurity states (e.g. Xe in Ar) the above cancellation may not be so complete because the potential of the impurity ion differs significantly from that of an ionized atom of the host crystal. Thus, because the Xe ion is larger than an Ar atom the excluded volume correction $\langle V_R \rangle$ outweighs the negative corrections $\langle V_{KE} \rangle$ and $\langle V_{DB} \rangle$, which are only slightly changed by the replacement of an Ar ion by a Xe ion, and the hydrogenic defect is large and positive[14,17]. In semiconductors, on the other hand, the valence shell is only half-filled and the excluded volume associated with the core is small. Thus (cf. I) the 1s donor binding energies are larger than the EMA result.

The model calculation has shown the relative magnitude of DB, KE, and R corrections to the macroscopic theory, and has led to a qualitative understanding of the success of

the EMA. However, the use of a differential equation to represent the Wannier equations is not valid for $\left(\frac{a_o}{a}\right)^2 \lesssim 1$;[18] in the calculation of deep states the finite spread of the Wannier function must be taken into account. We saw in section 3, for example, that certain two-center corrections are not negligible, and that calculated matrix elements differ significantly from $-e^2/\varepsilon_o R$ for $R \lesssim d$, the nearest neighbor destance. Consequently we must solve the Wannier equations (5.3); we do this by truncating and solving the secular equation. In the remainder of this section we present the results of calculations of 1s excitons in Kr and Xe; calculations of deep impurity states of Xe in Ne, Ar and Kr will be summarized in section 7.

Before solving the difference equations we recall that exciton states with $n \geq 2$ will not be given correctly by the solutions, because the curvature of our model energy bands is given incorrectly near $k = 0$ (cf. section 4). Since the 1s state will be orthogonal to these higher states, it is desirable to modify the equations in such a way that they are given correctly. We do this by renormalizing the macroscopic potential terms (3.19): we replace ε_o by $\varepsilon_o' = (\mu/\mu^*)^{1/2}\varepsilon_o$ ($\approx 1.3\,\varepsilon_o$ for Kr and Xe); for $R \lesssim d$ large-k behavior of the energy bands is important, and we retain the matrix elements of V_{ps}' listed in Table I.

The calculations show that the effective Bohr radius for 1s states is less than d, so that the replacement $\mathcal{E}_o \rightarrow \mathcal{E}'_o$ results only in slight modifications of the "tail" of the wave function.

Calculated hydrogenic defects for 1s excitons in Kr and Xe are listed in Table V. For comparison we list the defects obtained by neglecting the repulsive term V_R in the same table. The agreement between calculated and observed defects is excellent for the pseudopotential theory ($V = V_o + V_R$); the agreement is poor for $V = V_o$. Again, the occurrence of small defects is seen to be a consequence of the orthogonality requirement; the Schmidt terms in the impurity function $\psi(\underline{r}-\underline{R};)$ correspond to a large, positive kinetic energy which cancels the negative corrections (DB and KE).

The convergence of these results with respect to the number of basis functions is indicated in Figure 4 for Xe. R_c is the cut-off radius for the expansion of the model wave function φ in terms of Wannier functions. We note that the 1s energy has converged at $R_c \approx 3d$, while the larger 2s state must be expanded out to $R_c \approx 6d$ (40 shells) before convergence is indicated; the 2s energy appears to converge toward the experimental value of -0.23 eV.

Calculated 1s envelope functions are shown in Figures 6 and 7, along with the EMA function (6.1). Once again the

repulsive term V_R plays a fundamental role in the result; comparison of wave functions $A(V = V_o + V_R)$ and $B(V = V_o)$ illustrates the reduction of amplitude in the central cell brought about by the repulsive term V_R. In addition to diminishing the binding energy, this effect lowers the oscillator strength[19]

$$f_{ns} \sim |F_{ns}(0)|^2 \qquad (6.12)$$

In Table VI we list the ratio $r = f_{1s}/f_{2s}$ calculated from (5.3) and (6.12) ($R_c = 6d$) and compare with the hydrogenic prediction and experiment[13]. Because V_R reduces $F_{2s}(0)$ as well as $F_{1s}(0)$ the calculated ratio of oscillator strengths is nearly given by the EMA result. Agreement of the calculated ratio and experiment is excellent for Xe but not for Kr; in the latter case the experimental ratio is less certain because of greater lifetime broadening.

7. Deep Impurity States.

The availability of optical data[14,17] on the first excited states of a substitutional Xe impurity in crystals of Ne, Ar and Kr makes it possible to study the dependence of exciton binding on the macroscopic parameters ε_o and μ^*. For $n \geq 2$ this dependence is given by the hydrogenic formula

because the effective Bohr radii for these states are large compared with the atomic radius. For n = 1, on the other hand, there is only a weak dependence of binding energy on ε_o and μ^*, indicating that the wave function is confined to the neighborhood of the Xe impurity. Thus it is important that these deep states be calculated from the microscopic theory developed above; in this section we present the results of this calculation.

Hydrogenic defects of the first excited state (1s) of Xe were calculated for the systems (I) Xe in Ne, (II) Xe in Ar, (III) Xe in Kr, and (IV) pure Xe (cf. section 6). The results shown in Fig. 7 are plotted against the EMA binding energy $|E_H(1s)|$ and are normalized by the same factor. Comparison of curves A($V = V_o + V_R$) and B($V = V_o$) shows once again the crucial role played by the repulsive terms in the central cell. The agreement between the pseudopotential theory (curve A) and experiment is excellent over the entire range of interaction strength, from pure Xe, where $|E_H(1s)| = 0.86$ eV, to Xe in Ne, where $|E_H(1s)| = 2.59$ eV.

As expected (cf. section 6) the repulsive term outweighs the negative corrections to the EMA in I, II, and III, and large positive defects are observed; in IV the cancellation between central cell corrections is nearly exact.

The influence of the repulsive terms can be more clearly seen in the envelope functions. Solutions of the

difference equations for the 1s states are given in Figures 8 and 9. In both figures, the amplitude at the nearest neighbor site indicated by d_J increases relative to the amplitude at the origin as $\mathcal{C}_o$ decreases (i.e., as the interaction strength outside the central cell increases). In Figure 8 ($V = V_o$) all systems except I show enhanced amplitude at R = 0 relative to the hydrogenic value, because of DB and KE (negative) corrections to the binding energy. Figure 9 includes the effects of the repulsive term V_R in addition to the above corrections; $F_{1s}(0)$ is depressed compared to the hydrogenic value in all cases. Because of the latter reduction we expect the oscillator strength ratio $r = f_{1s}/f_{2s}$ to be less than the hydrogenic value (8:1) and that this ratio will increase with the atomic number of the host (i.e., as $F_{1s}(0)$ increases). Values of r computed from equation (6.12) using solutions of the Wannier equations for $R_c = 6d$ are given in Figure 10, together with values of this quantity estimated from the optical data by comparing the area under the absorption peaks for n = 1 and n = 2. Agreement between our pseudopotential theory and experiment is excellent for all cases. As expected, the reduction of r from the hydrogenic result is greatest for case I (Xe in Ne) where the ratio of impurity "volume" to the atomic volume of the host is largest.

8. Discussion.

We have applied the pseudopotential theory of exciton and impurity states developed in I to a calculation of (1) 1s excitons in Kr and Xe, and (2) 1s states of a Xe impurity in Ne, Ar and Kr. Three corrections to the hydrogenic theory were considered: (a) dielectric breakdown, (b) large-k variation of the effective mass, and (c) repulsive terms in the central cell, representing core parts of the impurity function. To determine the relative magnitude of each effect a model Hamiltonian based on simple interpolation formulae was constructed. First-order corrections to the hydrogenic theory were calculated; the total energy shifts agreed in sign with the experimental shifts. Because each contribution (a) - (c) could be evaluated separately it was possible to obtain a qualitative understanding of the remarkable success of the effective mass approximation for excitons in Kr and Xe. Specifically, it was shown that the positive correction due to the effective repulsive potential cancels the negative contributions (a) and (b) to a large extent, with the result that the hydrogenic defect is small.

In order to verify the results of the model calculation the Wannier difference equations were solved by a matrix technique. The calculated binding energies and oscillator strengths were in excellent agreement with experiment in

all cases. To our knowledge this is the first time that the Wannier wave-packet approach has been shown to yield good results for deep states in insulating crystals. From our results one may conclude that the neglect of exchange and local field corrections to the electron-hole interaction is justified, and non-local terms in the exciton Hamiltonian may be neglected. Finally, the representation of the energy bands by our simple interpolation formula does not produce serious errors. (With additional computational effort and at the expense of simplicity it would be possible to improve further the treatment of the kinetic energy terms.) Thus, if we were to choose a smaller bandwidth for Ar or Kr (as Mattheiss' APW calculations[20] have suggested) the enhanced density of states at the interband threshold would lead to stronger binding and, consequently, better agreement with experiment. We note that our calculations for Xe and Ne, for which the band structure is more certain (cf. section 4), are in essentially exact agreement with experiment--even the anomalous oscillator strength ratio for Ne (2:1 rather than 8:1) is given correctly.

The success of our calculations for parabolic excitons indicates that the electron-hole potential we constructed is good over the entire range of r. Thus we are in a position to calculate excitons derived from higher conduction bands[21,22] as well as scattering resonances associated with

critical points in the interband density of states that lie above the fundamental edge. Phillips[23] has suggested that peak structure observed in the insulators above threshold may often be interpreted in terms of such resonances. Calculations based on this suggestion are being carried out by the author.

Extension of the methods of this paper to the alkali halides is straightforward. The conduction bands of the two systems are similar, so that the treatment of kinetic energy terms needs only slight modification (viz., inclusion of a width for the halide valence bands). From the results of this paper one would anticipate that exciton states in the alkali halides should follow a hydrogenic pattern, especially in those crystals, such as KBr, RbBr, KI, and RbI, whose bands closely resemble those of the solid rare gases[10].

FIGURE CAPTIONS

Fig. 1. Dielectric function of Argon (atomic units). The solid line is our model for an isotropic insulator, based on a parabolic excitation spectrum. For purposes of comparison, Penn's model for an isotropic semiconductor is shown by the dashed line (based on parameters appropriate to Ar). The "breakdown length" Q^{-1} for the insulator dielectric function is less than the atomic radius of Ar (3.55 a.u.).

Fig. 2. Unscreened pseudopotential for excitons in Xe. The solid curve was obtained from the Hartree potential by the projection technique of Cohen and Heine. $\gamma = r_o/a$ measures an average radius r_o of the excluded volume relative to the atomic radius a. The value of r_o is defined by the requirement that the average of the pseudopotential from 0 to r_o be zero.

Fig. 3. Band structure of Xe, as inferred from optical data. The double-group notation is used for the valence bands, the single-group for the conduction bands.

Figure Captions (continued)

Fig. 4. Convergence of exciton energies for Xe. R_c is the cut-off radius defined in the text. The observed energies of the 1s and 2s states are given by the dashed lines A. and B. For $R_c \longrightarrow \infty$ a rydberg series for $n \geq 2$ is expected.

Fig. 5. Envelope function for 1s exciton in Kr. The hydrogenic envelope function is given by the dashed line. The solid curves are solutions of the difference equations for n = 1. Curve A includes the effects of the repulsive potential while curve B does not. The nearest-neighbor distance is d.

Fig. 6. Envelope function for 1s exciton in Xe. The notation is the same as Figure 5.

Fig. 7. Relative hydrogenic defects of the 1s state of a Xe impurity in various host lattices. The abcissa is $|E_H(1s)|$, the hydrogenic binding energy, which is a measure of the strength of the electron-hole coupling neglecting central cell corrections. Experimental defects are joined by the dashed line; theoretical curve A passes close to the experimental shifts. Curve B indicates the re-

Fig. 7. (continued)

sults obtained without the repolsive potential V_R. The agreement between theory and experiment is qualitatively poor for curve B, which predicts that the hydrogenic defect is always negative.

Fig. 8. Envelope function for the 1s state of a Xe impurity in various rare gas host lattices. Orthogonality corrections to the impurity potential were neglected ($V = V_o$) in these calculations. The dashed line is the hydrogenic envelope function for the 1s exciton in Xe and d_J is the nearest-neighbor distance in the J^{th} system.

Fig. 9. Envelope function for the 1s state of Xe in various host lattices, calculated with the pseudopotential $V = V'_{ps} = V_o + V_R$. Note that the central cell amplitude is reduced from Fig. 8, due to the repulsive term V_R.

Fig. 10. Oscillator strength ratio for a Xe impurity in several rare gas environments. $r = (f_{1s}/f_{2s})$ is given by the ratio of central cell amplitudes for n = 1 and n = 2. According to the hydrogenic

Fig. 10. (continued)

theory r has the constant value 8.0 independent of environment. Curve A was obtained by solving the Wannier equations with $V = V'_{ps} = V_o + V_R$, and the experimental results are given by the dashed line. The disagreement between theory and experiment for Xe in Ar and Xe in Kr is thought to be due primarily to uncertainties in the band structures assumed for these crystals.

TABLE CAPTIONS

Table I. Matrix elements of the potential in eV between Wannier functions either in the central cell, $|0\rangle$, or the nearest neighbor, $|d\rangle$. The primary numbers refer to the pseudopotential, whereas the numbers in parentheses refer to the crystal potential ($V_R = 0$). For comparison the magnitude of the screened Coulomb potential at the nearest neighbor sites is shown in the last column.

Table II. Microscopic parameters used to determine chemical shifts in conduction band models for the family of rare gas solids.

Table III. Microscopic parameters for Kr and Xe (atomic units) in simplified quasi-hydrogenic model.

Table IV. Energy shifts of 1s excitons in Kr and Xe (in units of $|E_H(1s)| = \frac{\mu^* e^4}{2\varepsilon_o^2 \hbar^2}$) as computed from simplified model. The terms $\langle V_{DB} \rangle$, $\langle V_{KE} \rangle$ and $\langle V_R \rangle$ are defined in the text. The sum of the first two gives an estimate ΔE_{KL} of the hydrogenic defect according to the Kohn-Luttinger methods (ref. 16). The sum of all three terms gives ΔE. The relative hydrogenic defects

Table IV. (continued).

observed experimentally are given in column 6.

Table V. Hydrogenic defects of 1s excitons in Kr and Xe obtained from the Wannier equations relative to $|E_H(1s)|$. The first column contains results for $V_R = 0$. Results obtained with the pseudopotential $V'_{ps} = V_o + V_R$ are given in column two, and the experimental results are listed in column three.

Table VI. Oscillator strength ratio $r = f_{1s}/f_{2s}$ for excitons in Kr and Xe. The first column contains the hydrogenic value, and columns two and three contain results obtained from the Wannier difference equation for $V = V_o$ and $V = V_o + V_R$, respectively. The last column lists values of r deduced by Baldini.

	System	$\langle o\|V\|o \rangle$	$\langle o\|V\|d \rangle$	$\langle d\|V\|d \rangle$	$-e^2/\epsilon_o d$
1.	Xe in Ne	-1.03 (-4.47)	-0.01 (-0.24)	-3.34 (-4.16)	-4.12
2.	Xe in Ar	-1.28 (-3.75)	-0.13 (-0.30)	-1.98 (-2.78)	-2.31
3.	Xe in Kr	-1.38 (-3.51)	-0.15 (-0.28)	-1.74 (-2.46)	-1.99
4.	pure Xe	-1.43 (-3.17)	-0.15 (-0.27)	-1.25 (-1.89)	-1.47
5.	pure Kr	-2.18 (-4.24)	-0.225 (-0.35)	-1.84 (-2.57)	-1.99

Table I.

Element	f_o(a.u.)	S_L(eV)	E_L(eV)	$(\mu^*/m)^x$	$(\mu/m)^y$
He	1.19	--	--	--	--
Ne	0.24	0	5.6	--	0.40
Ar	-1.70	0.4	3.8	0.46	0.43
Kr	-3.7	0.8	3.1	0.41	0.46
Xe	-6.5	1.4	2.2	0.31	0.54

[x] Deduced by Baldini from rydberg series for $n \geq 2$.

[y] From curvature of our model $W(\underline{k})$ near $k = 0$.

Table II.

Crystal	Q(DB)	$a^{-1}(KE)$	$\gamma = r_o/A$ (R)
Kr	0.6	.094	0.80
Xe	0.5	.086	0.86

Table III.

Crystal	$\langle V_{DB} \rangle$	$\langle V_{KE} \rangle$	$\langle V_R \rangle$	ΔE_{KL}	ΔE	ΔE_{exp}
Kr	-0.06	-0.55	+0.92	-0.61	+0.31	+0.13
Xe	-0.07	-0.51	+0.53	-0.58	-0.05	-0.07

Table IV.

Crystal	$\Delta E(V = V_o)$	$\Delta E(V = V_o+V_R)$	$\Delta E(exp)$
Kr	-0.80	+0.15	+0.13
Xe	-1.76	-0.09	-0.07

Table V.

Crystal	r(EMA)	r($V = V_o$)	r($V = V_o+V_R$)	r(exp)
Kr	8	10.7	8.0	4.0
Xe	8	11.0	9.0	9.0

Table VI.

REFERENCES

1. J. Hermanson and J. C. Phillips (preceding paper), referred to as I in this paper.
2. N. Wiser, Phys. Rev. 129, 62 (1963).
3. J. C. Phillips, Phys. Rev. 136, A1714 (1964).
4. D. R. Penn, Phys. Rev. 128, 2093 (1962).
5. H. Nara, Phys. Soc. Jap. 20, 778 (1965).
6. P. Nozieres and D. Pines, Phys. Rev. 109, 741 (1958).
7. W. Kohn, Phys. Rev. 110, 857 (1958).
8. M. H. Cohen and V. Heine, Phys. Rev. 122, 1821 (1961).
9. F. Herman and S. Skillman, Atomic Structure Calculations (Prentice-Hall, Inc. 1963).
10. J. C. Phillips, Phys. Rev. 136, A1705 (1964).
11. N. Ashcroft, Phys. Rev. 140, A935 (1965).
12. T. F. O'Malley, Phys. Rev. 130, 1020 (1963).
13. G. Baldini, Phys. Rev. 128, 1562 (1962).
14. G. Baldini, Phys. Rev. 137, A508 (1965).
15. W. Kohn and J. M. Luttinger 98, 915 (1955).
16. W. Kohn, SSP 5, 257 (1957).
17. G. Baldini and R. S. Knox, Phys. Rev. Letters 11, 127 (1963).
18. E. N. Adams, Phys. Rev. 85, 41 (1952).

References (continued)

19. R. J. Elliott, Phys. Rev. 108, 1384 (1957).

20. L. F. Mattheiss, Phys. Rev. 133, A1399 (1964).

21. A. W. Overhauser, Phys. Rev. 101, 1702 (1956).

22. R. S. Knox and N. Inchauspe, Phys. Rev. 116, 1093 (1959).

23. J. C. Phillips, Phys. Rev. Letters 12, 142 (1964).

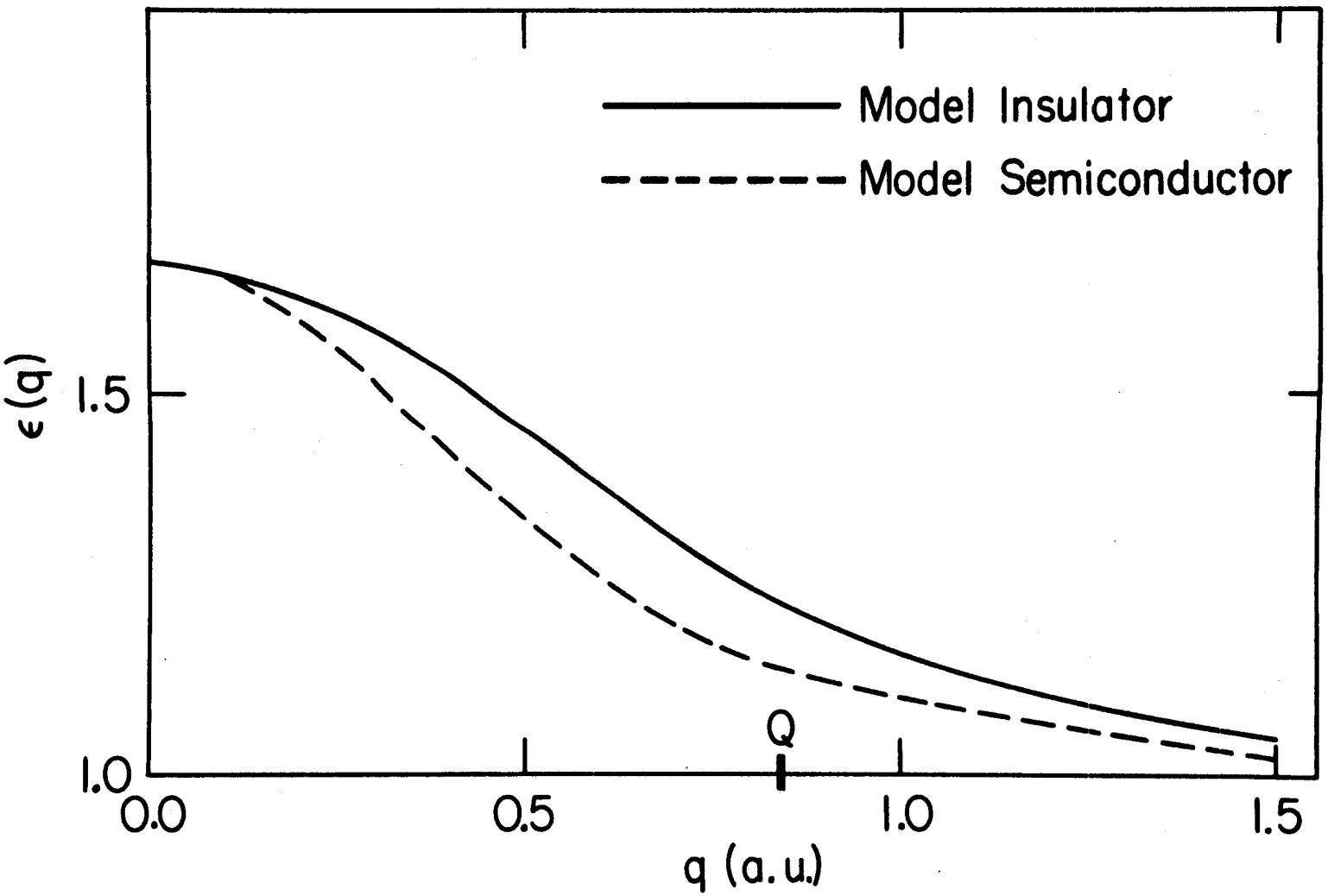
Model Insulator
Model Semiconductor
ε(q)
1.5
1.0
Q
0.0
0.5
1.0
1.5
q (a.u.)

Fig. 1

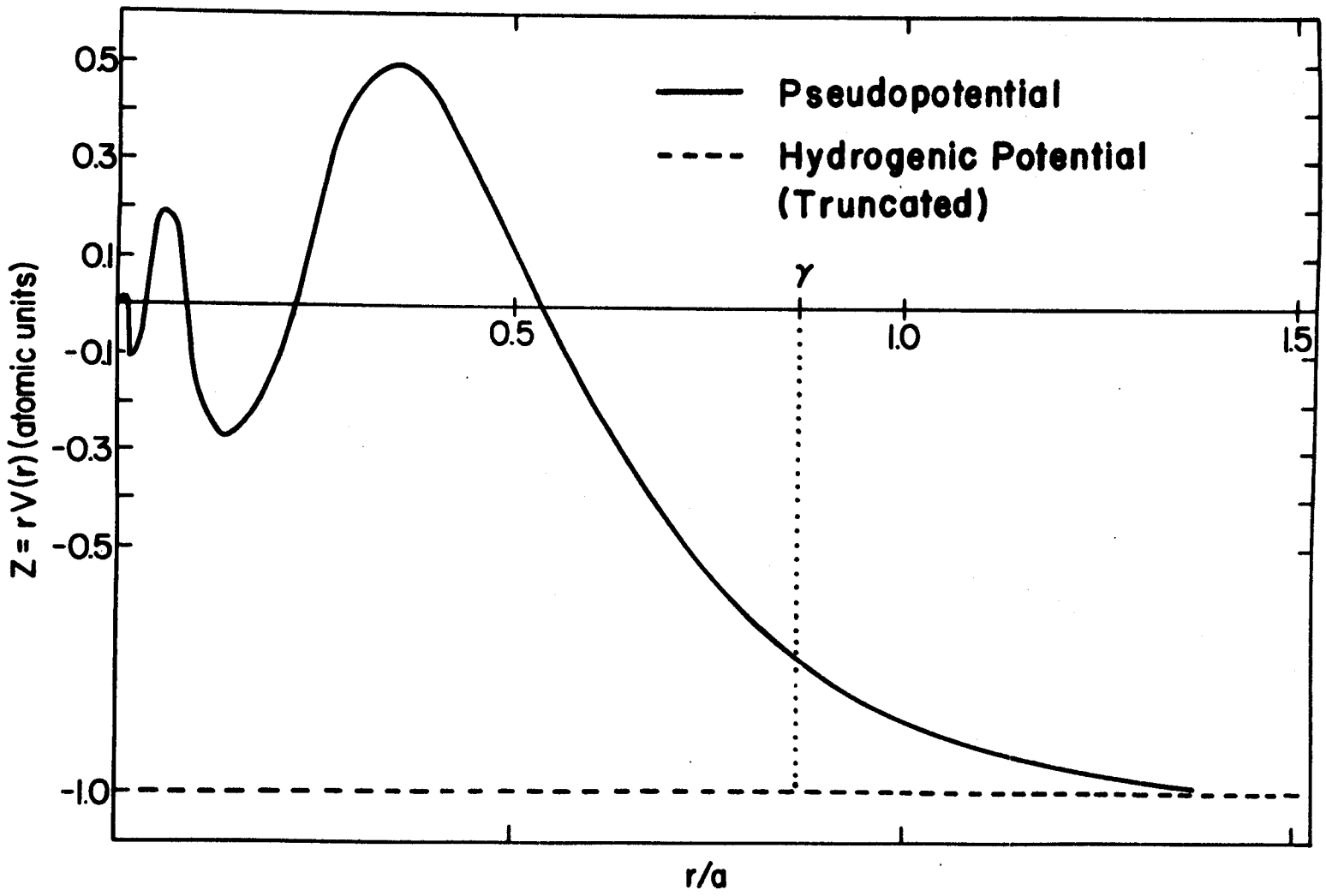
0.5
0.3
0.1
-0.1
-0.3
-0.5
-1.0
0.5
1.0
1.5
γ
Pseudopotential
Hydrogenic Potential
(Truncated)
Z = rV(r) (atomic units)
r/a

Fig. 2

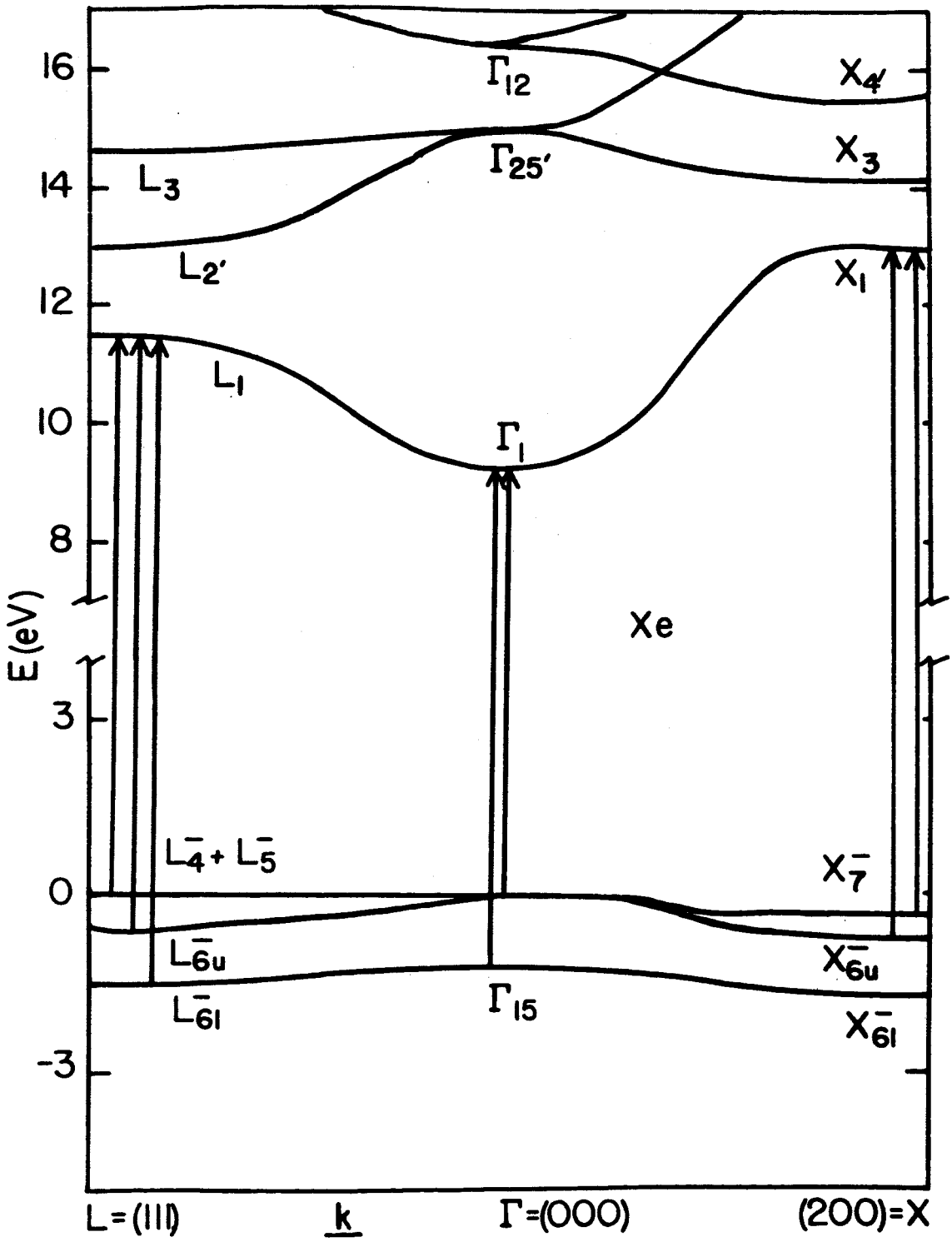
16
14
12
10
8
3
0
-3
E(eV)
Γ_{12}
$X_{4'}$
$\Gamma_{25'}$
X_3
L_3
$L_{2'}$
X_1
L_1
Γ_1
Xe
$L_4^- + L_5^-$
X_7^-
L_{6u}^-
X_{6u}^-
L_{61}^-
Γ_{15}
X_{61}^-
L=(111)
k
Γ=(000)
(200)=X

Fig. 3

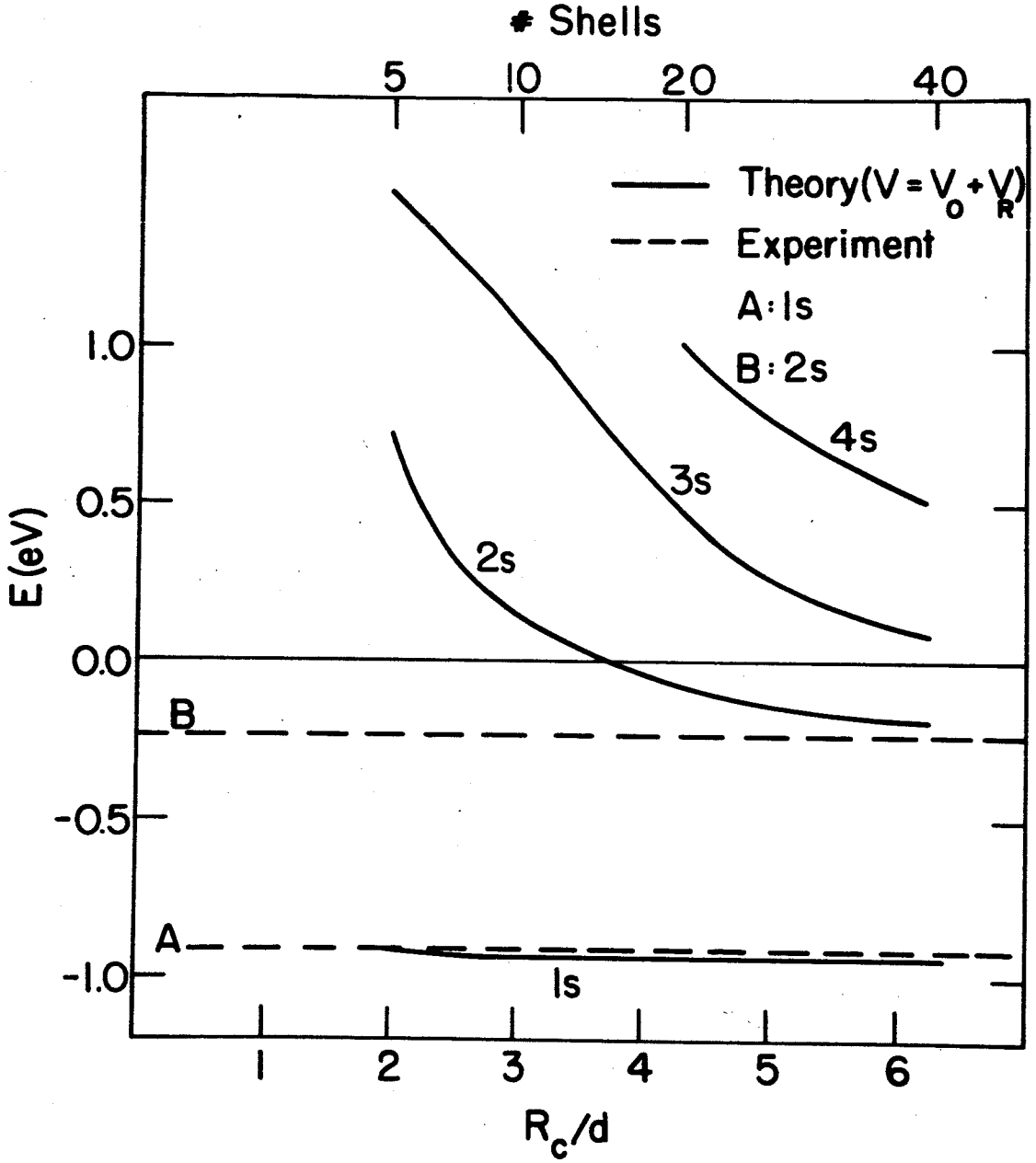
Shells
5
10
20
40
Theory($V = V_o + V_R$)
Experiment
A: 1s
B: 2s
4s
3s
2s
1.0
0.5
0.0
-0.5
-1.0
E(eV)
B
A
1s
1
2
3
4
5
6
R_c/d

Fig. 4

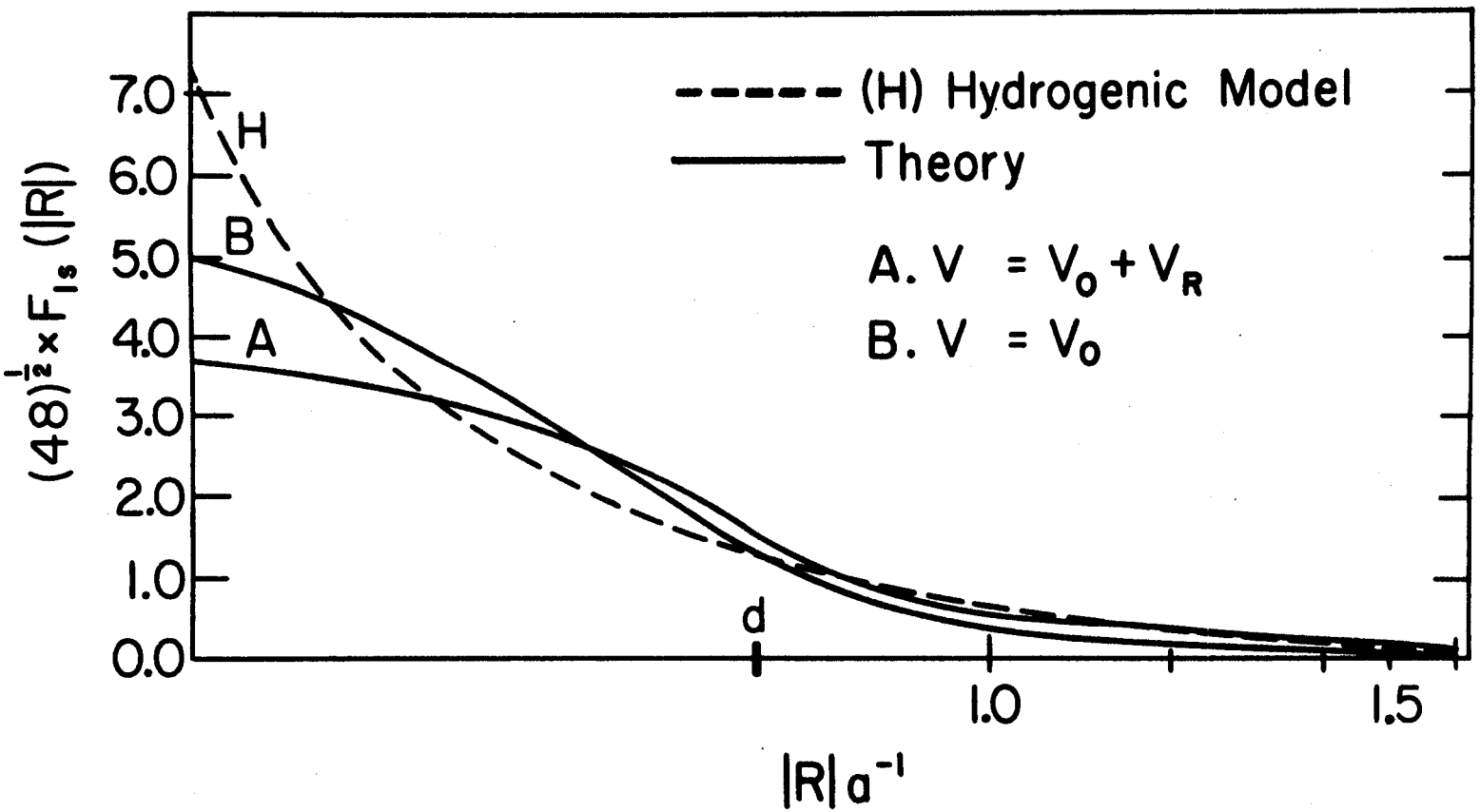
(H) Hydrogenic Model
Theory
A. V = V0 + VR
B. V = V0
H
B
A
7.0
6.0
5.0
4.0
3.0
2.0
1.0
0.0
d
1.0
1.5
(48)^½ × F1s (|R|)
|R| a^-1

Fig. 5

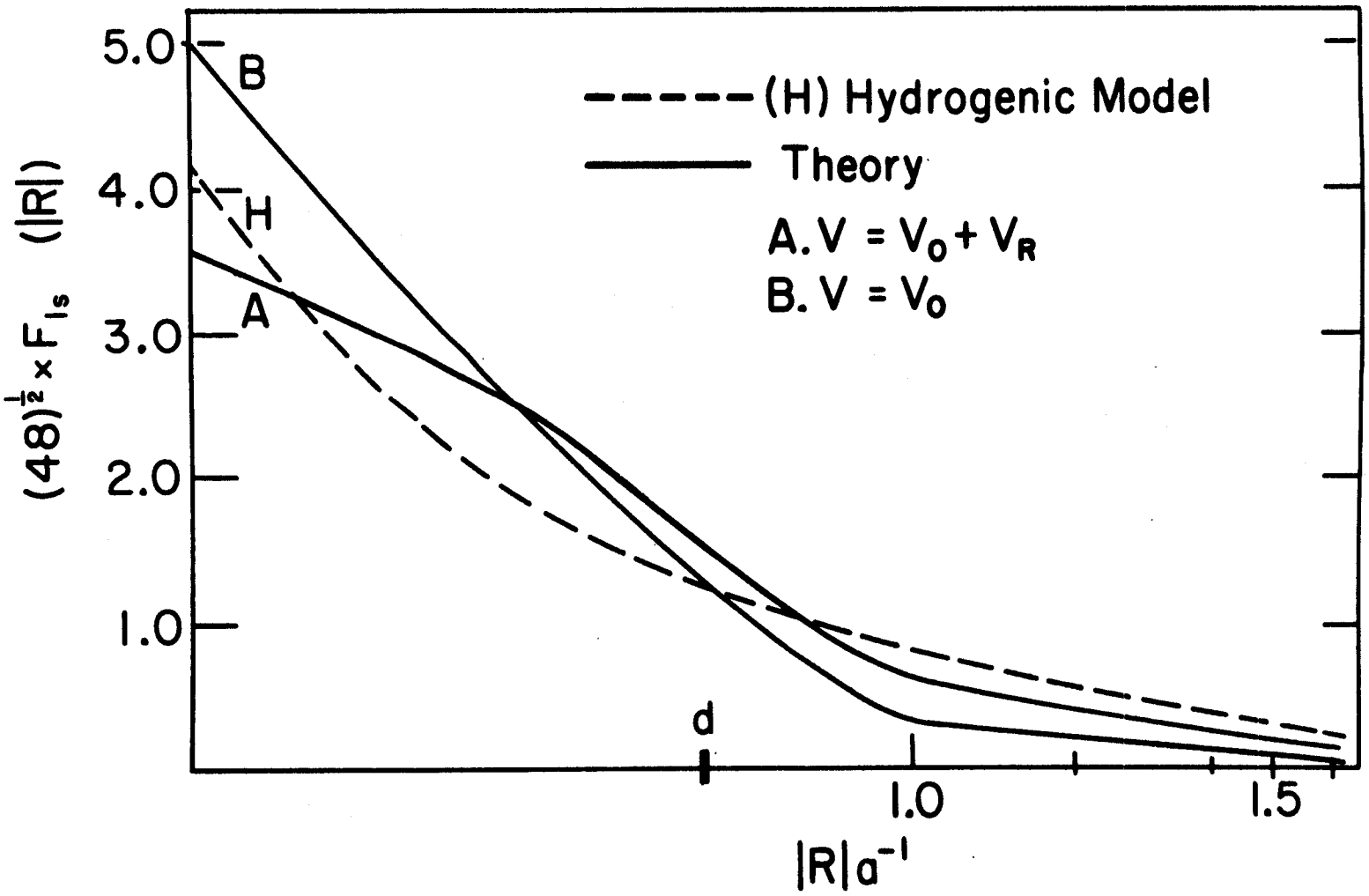
5.0
4.0
3.0
2.0
1.0
B
H
A
(H) Hydrogenic Model
Theory
A. V = V0 + VR
B. V = V0
d
1.0
1.5
|R|a-1
(48)½ x FIs (|R|)

Fig. 6

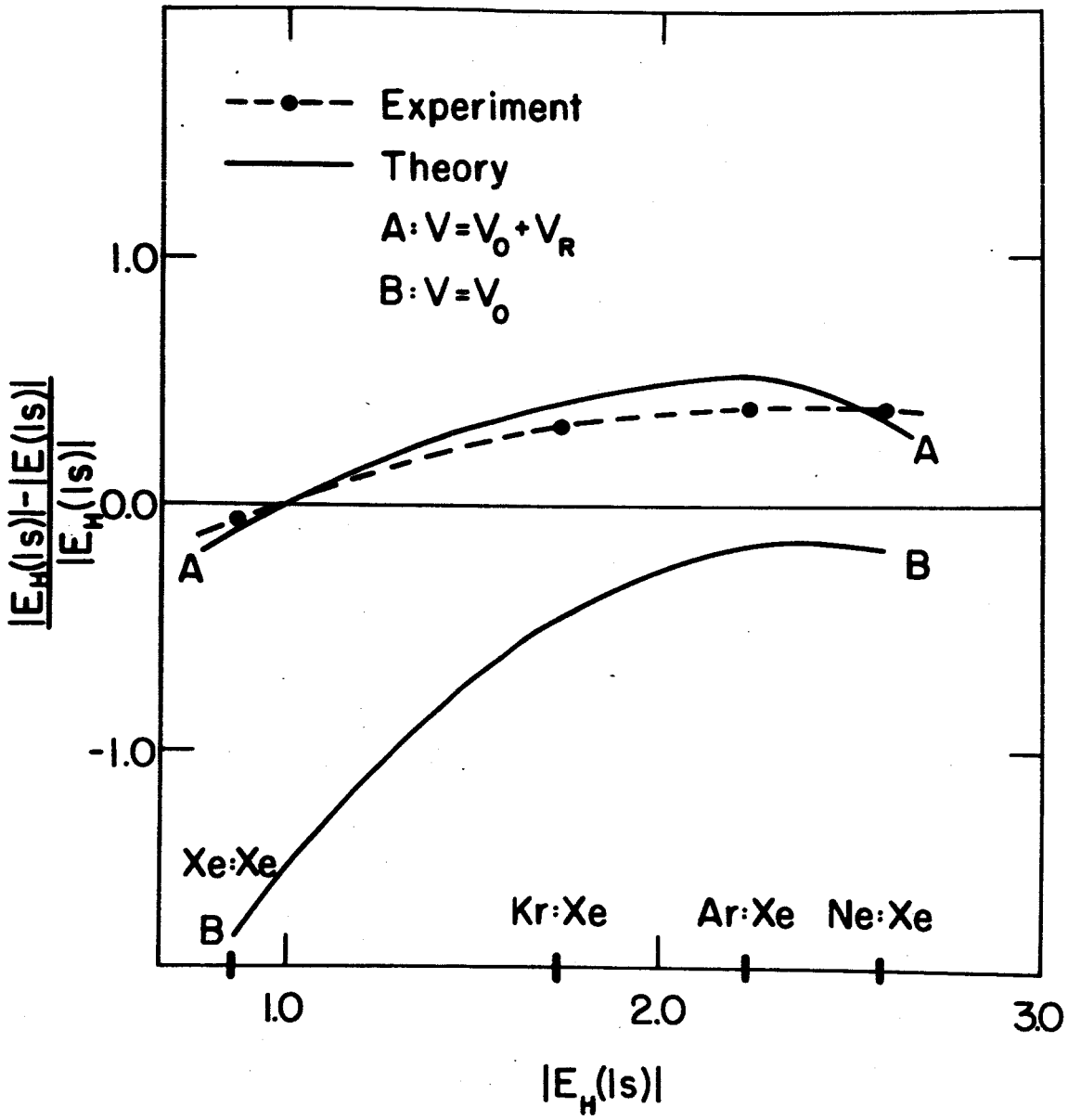
Experiment
Theory
A: V=V0+VR
B: V=V0
1.0
0.0
-1.0
A
A
B
B
Xe:Xe
Kr:Xe
Ar:Xe
Ne:Xe
1.0
2.0
3.0
|EH(ls)|
|EH(ls)|-|E(ls)| / |EH(ls)|

Fig. 7

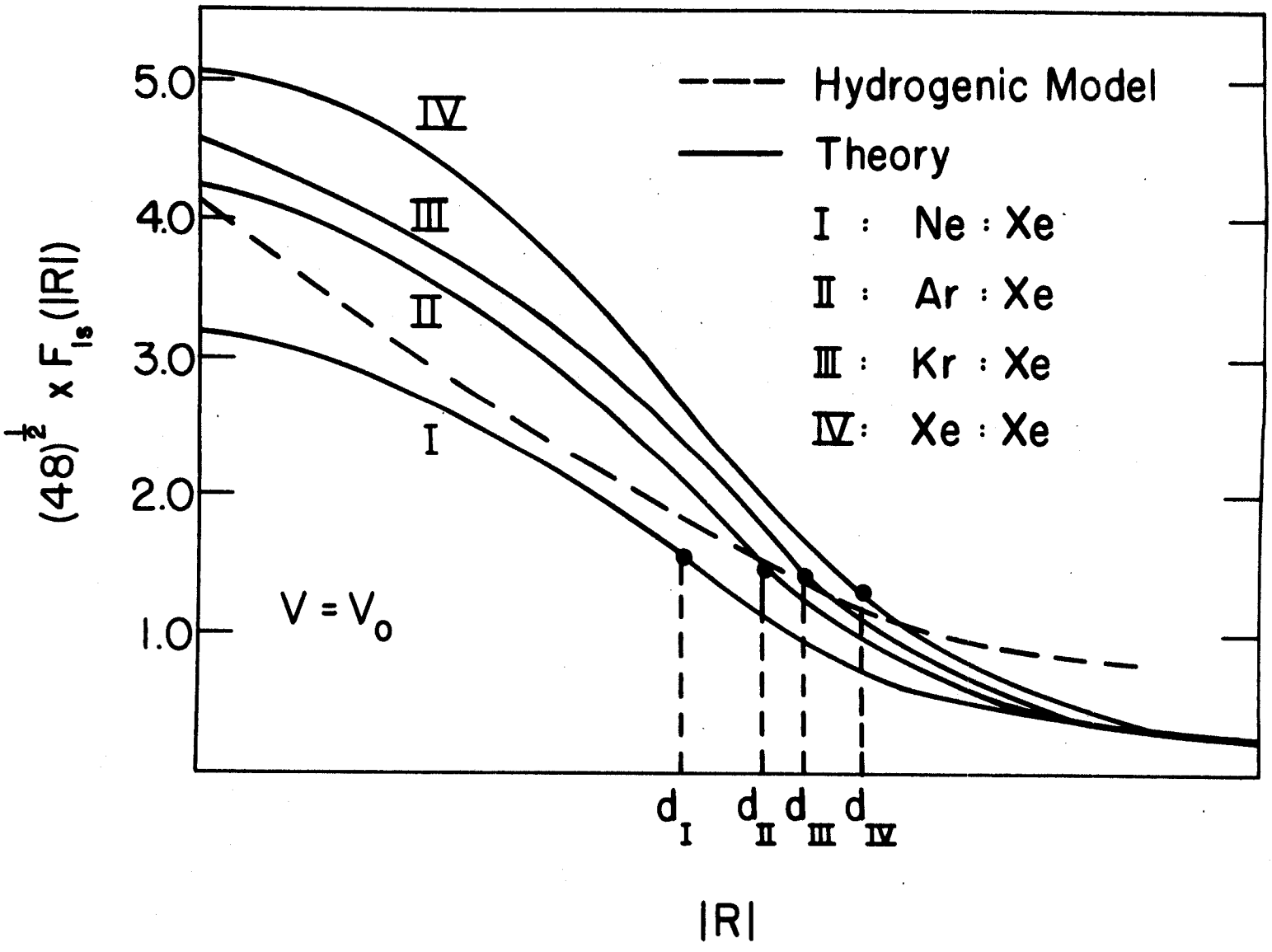
Hydrogenic Model
Theory
I : Ne : Xe
II : Ar : Xe
III : Kr : Xe
IV : Xe : Xe
5.0
4.0
3.0
2.0
1.0
$(48)^{\frac{1}{2}} \times F_{1s}(|R|)$
$V = V_0$
d_I d_{II} d_{III} d_{IV}
|R|

Fig. 8

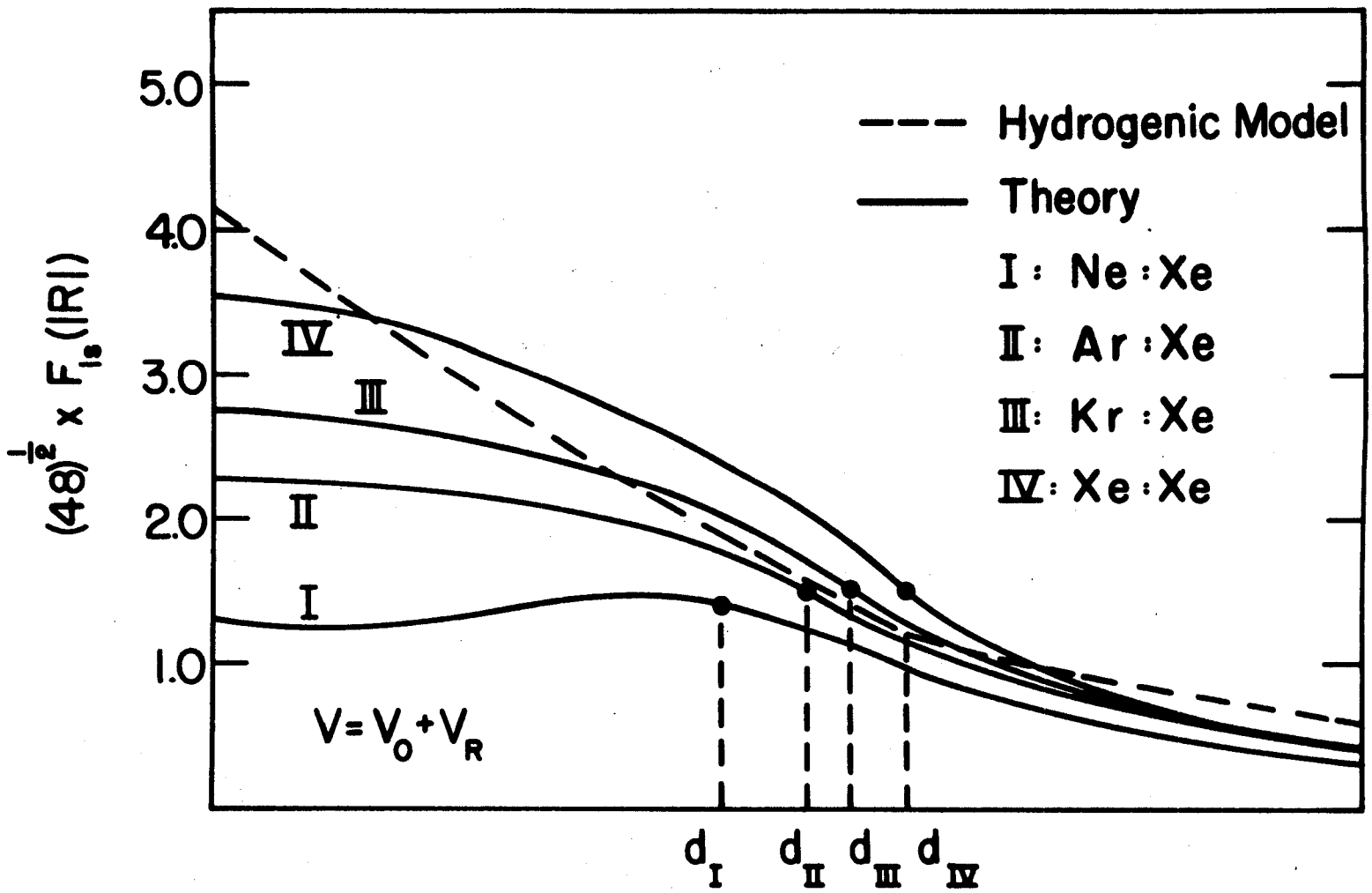
5.0
4.0
3.0
2.0
1.0
$(48)^{\frac{1}{2}} \times F_{1s}(|R|)$
Hydrogenic Model
Theory
I : Ne : Xe
II : Ar : Xe
III : Kr : Xe
IV : Xe : Xe
IV
III
II
I
$V = V_0 + V_R$
d_I d_{II} d_{III} d_{IV}
|R|

Fig. 9

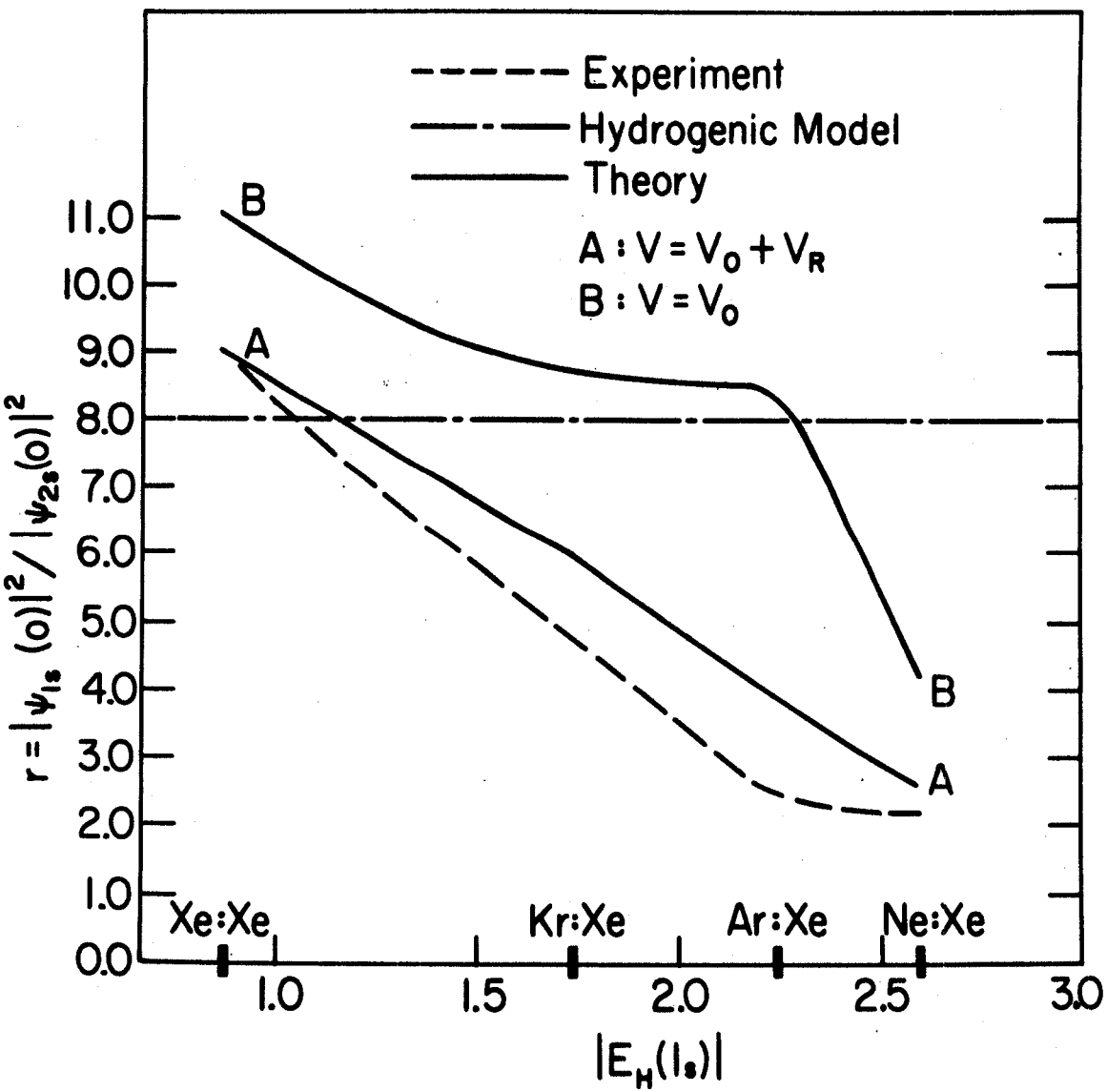
Experiment
Hydrogenic Model
Theory
A : V = V0 + VR
B : V = V0
B
A
B
A
11.0
10.0
9.0
8.0
7.0
6.0
5.0
4.0
3.0
2.0
1.0
0.0
r = |ψ1s (0)|2 / |ψ2s(0)|2
Xe:Xe
Kr:Xe
Ar:Xe
Ne:Xe
1.0
1.5
2.0
2.5
3.0
|EH(1s)|

Fig. 10